



Turbulent Natural Convection in an Enclosure at Varying Rayleigh Number

Stephen Karanja^{a*}, Johana Sigey^b, Francis Gatheri^c, Eustace Kirima^d

^{a,d}*Department of Mathematics, Meru University of Science and Technology, P.O Box 972-60200, Meru, Kenya.*

^b*Department of Pure and Applied Mathematics, Jomo Kenyatta University of Agriculture and Technology, P.O Box 60000-00200, Nairobi, Kenya.*

^c*School of Mathematics and Actuarial Science, Technical University of Kenya, P.O Box52428-00200, Nairobi, Kenya.*

^a*Email: stephenkaranja16@gmail.com*

^b*Email: jksigey@jkuat.ac.ke*

^c*Email: kgatheri@gmail.com*

^d*Email: emwenda@must.ac.ke*

Abstract

Most fluids used in technical applications are of low viscosity; hence, fluid flows encountered in engineering applications are mostly turbulent. Parameters that influence the distribution of the flow field of turbulent flow regimes thus significantly affect the performance of many thermal systems. In this study, we analyze the distribution of the flow field of a Boussinesq buoyancy-driven turbulent airflow for $10^9 \leq Ra < 10^{11}$ and $Pr = 0.71$, and establish the effect of the Rayleigh number on these distributions. The flow domain comprises of a rectangular enclosure of constant aspect ratio, partially heated on a sidewall and cooled on the opposite wall. Due to the rapid fluctuations in flow properties intrinsic in the turbulent flow regime, we subject the equations governing a viscous incompressible buoyant fluid flow to the Reynolds decomposition and averaging process to obtain equations that describe a turbulent flow field. We treat turbulence using the *SST* $k - \omega$ turbulence model coupled with the Boussinesq approximation.

* Corresponding author.

To ensure that the conservation laws are satisfied at both the local and over the entire flow domain, the equations are discretized using the robust finite volume method. The method possesses the ability to adapt a grid structure that captures the local features of the flow domain and the final form of the discretized equations has an intimate connection to the actual physical laws. Since the equations are coupled, a segregated pressure-based iterative method is used to obtain the solution. The results obtained revealed that the flow fields are distributed non-uniformly in the flow domain and the distribution significantly depend on the Rayleigh number of the flow. The results are consistent with the experimental results of Markatos and Pericleous (1984).

Keywords: Buoyancy; Natural Convection; Reynolds Stresses; Turbulent heat flux; Turbulence Modeling.

1. Introduction

In most confined fluid flows accompanied by energy transfer, the primary mode of heat transfer is natural convection caused by a heat source at some location in the flow domain. In addition, in thermal systems comprising multimodal heat transfer mechanisms, natural convection is the dominant mode of heat transfer, moreover, when it is desirable to minimize the cost of operation, natural convection is often the preferred means of heat transfer. Consequently, in many thermal systems encountered in engineering applications, energy transfer mechanism is mainly through natural convection. Therefore, parameters that influence the rate of heat transfer in natural convective flows significantly affect the performance of many thermal systems. Heat transfer in natural convective flow regimes thus enjoys a noticeable interest from the thermal sciences community [1]. In this flow regime, the coefficient of heat transfer is dependent on the thermal properties of the fluid, flow conditions and the geometry of the flow domain [2]. Consequently, for a confined buoyancy-driven fluid flow in a flow domain of constant aspect ratio, the characteristics of the flow field significantly depend on the properties of the fluid and the thermal conditions of the confining walls.

In natural convective flows, the Rayleigh number, named after Lord Rayleigh is indicative of the strength of the buoyancy force that initiates and sustains the flow. The force is due to density variations associated with temperature gradients within the flow domain. The Rayleigh number is thus a function of the thermal conditions of the confining walls and the coefficient of volumetric expansion of the fluid. The Rayleigh number thus incorporates the properties of the fluid and the flow conditions into a single parameter. This non-dimensional number therefore dictates the mechanism of heat transfer. For $Ra \leq 10^4$, heat transfer mechanism is primarily by conduction whereas for $10^4 < Ra < 10^9$ heat transfer is predominantly by laminar natural convection. For $Ra \geq 10^9$, the transfer of heat is principally through turbulent natural convection [2].

Most fluids used in technical applications are of low viscosity; consequently, fluid flows encountered in engineering applications are mostly turbulent. In order to meet the ever-increasing need of enhancing the energy-efficacy of thermal systems, the determination of the influence of the Rayleigh number on the distribution of the flow field in a turbulent natural convective flow is thus a worthwhile endeavor. To examine the effects of the rapid fluctuations inherent in the turbulent flow regime on the flow field, we subjected the equations governing a Newtonian viscous incompressible buoyant fluid flow to the Reynolds decomposition and averaging process to obtain equations governing a turbulent flow field. The averaging process however

introduced unknown non-linear terms associated with the turbulence of the flow. The determination of these terms poses the greatest challenge in the analysis of the turbulent flow regime [3]. However, due to its enormous practical importance, the need of analyzing this flow regime is inevitable. To meet this need, we used the Shear Stress Transport $k-w$ turbulence model developed by Menter in 1994 coupled with the Boussinesq approximation to resolve the turbulence and the robust finite volume method to discretize the equations. The results are applicable in locally heated and cooled thermal systems in determining the flow conditions that ensures that the distribution of the flow fields optimally meets the thermal requirements of the user. However, they are not applicable for laminar and forced convection flows.

1.1 Review of Previous Related Studies

Turbulent natural convection in confined flow domains arising from partly heated walls is receiving increasing research attention due to its many practical applications in the real world. In 1883, Osborne Reynolds carried out the first systematic work on turbulence in his pipe flows experiments. He asserted that a fluid flow becomes turbulent when a non-dimensional number named the Reynolds number by Sommerfeld, exceeds a certain critical value [5]. This non-dimensional number has since then been the parameter that determines the dynamic similarity of viscous flows. He also introduced the concept of decomposition and averaging in 1895 in which he expressed a flow property in a turbulent flow field as a sum of a mean and fluctuation value. These discoveries by Reynolds have proved to be of fundamental importance in the analysis of the turbulent flow regime. Since then, researchers have conducted a significant number of experimental and numerical studies in an attempt to demystify this complex flow regime.

In 1985, the authors in reference [6] carried out a numerical study using the $k-\varepsilon$ turbulence model in a cubical water-filled enclosure heated and cooled isothermally on opposite vertical walls with all other walls insulated. They studied the flow profiles of both laminar and turbulent natural convection in the enclosure for $10^6 \leq Ra \leq 10^8$ and $10^9 \leq Ra \leq 10^{11}$ for the laminar and turbulent flow respectively. The results showed that the numerical analyzes of the laminar flow regime were consistent with the experimental results of Churchill and Usagi. They also revealed the sensitivity of the parameters used in the adopted $k-\varepsilon$ turbulent model. Results of a numerical analysis of turbulent natural convection in a cubical enclosure heated from below and locally cooled on the side was reported by the authors in reference [7] in 1986. They heated the entire floor of the enclosure and insulated all other walls. Using the $k-\varepsilon$ turbulence model, they computed three-dimensional isotherms and velocity vector plots for $10^6 \leq Ra \leq 10^7$ and $Pr = 0.7$. The results comprised of velocity vector plots in vertical planes both normal and parallel to the locally cooled sidewall and the distribution of the isotherms in the enclosure. Since experimental results under similar conditions were then unavailable, they did not validate the results.

In 1987, the authors in reference [8] used a numerical model to analyze a steady natural convection flow in a water-filled square enclosure locally heated from below and cooled on a sidewall using the finite difference method on a uniform 61×61 mesh. They varied the ratio of the heated area to the unheated area of the floor

and computed temperature contours for different proportions of the heated area for $Ra \leq 10^6$. They reported the dependence of the Nusselt number and heat transfer coefficient on the ratio of the heated area. However, it was not clear whether the model is applicable for $Ra > 10^6$. In the same year, the authors in reference carried [9] out an experimental study of natural convection in a water-filled rectangular enclosure consisting of a vertical wall halfway heated and half cooled such that the heated and cooled regions were vertically adjacent to each other. The objective of the study was to determine heat transfer and temperature field inside the enclosure for $Ra = 2.9 \times 10^{10}$ and $Ra = 4.6 \times 10^{10}$. They presented the results in form of isotherms maps on various vertical planes. The results showed that temperature distribution was qualitatively the same on both sides of the enclosure. In addition, they observed two boundary layers moving at the same rate side by side inside the enclosure. The warm layer was moving upwards whereas the cold layer moved downwards. However, there was no significant interaction between these layers.

The authors in reference [10] developed a numerical analysis of laminar flow in a cubicle enclosure locally heated and locally cooled at different positions in 1988. They performed an analysis of temperature and velocity distribution for four sets of heater and cooler positions with the heater position fixed for $Ra \leq 5 \times 10^5$ using the finite difference method coupled with the stream function-vorticity formulation and the false transient method. The results showed that the enclosure was unstably thermal stratified. Although the boundary conditions considered were similar to many real-life situations, the range of the Rayleigh number considered was too low for practical applications. In 1993, the authors in reference [11] carried out a numerical study to investigate turbulent flow in a three-dimensional rectangular enclosure containing a convective heater built into one vertical wall and a window mounted on the same wall but above the heater. The position of the center of the window was invariant but its size varied whereas the position and size of the heater remained unchanged. They solved the time-averaged equations of continuity, momentum and energy coupled with the transport equations of the turbulent scalar quantities using the vorticity-vector potential formulation method. The results revealed that the upper region of the enclosure was cold but the region between the heater and the window was hot whereas the lower region was warm. From the results, it was evident that heat transfer rate increased with the size of the window and the Rayleigh number of the flow.

The authors in reference [12] developed a numerical study for natural convection airflow in a two dimensional rectangular enclosure locally heated from below and cooled symmetrically from the sidewalls for Rayleigh number between $10^3 \leq Ra \leq 10^6$. They investigated the influence of the length of the heated portion on the flow field and heat transfer rate. A heater placed centrally at the bottom of the enclosure simulated the localized heating. They considered the dimensionless length of the heated surface of 0.2, 0.4, 0.6 and 0.8. The results showed that the average Nusselt number at the heated portion increases with the Rayleigh number and the temperature fields were symmetrical about the mid-width of the enclosure. In 2010, the authors in reference [13] carried out a numerical analysis of buoyancy driven free convection turbulent heat transfer in a three-dimensional rectangular enclosure consisting of a convective heater fixed in one of the sidewalls and a window mounted above the heater with all other walls insulated. They solved the equations governing natural convection using a fast and stable finite difference approximation method that they developed and validated coupled with the vorticity-vector potential formulation. The use of false transient factors in different locations of

the flow domain fastened convergence of the numerical solution. To treat turbulence, they employed the low-Reynolds number $k - \varepsilon$ model due to its high accuracy in the free stream regions. They noticed two boundary layers that collided in the region between the window and heater. The results showed that the region between the heater and the window was hot while the upper region was cold. However, the lower region of the enclosure was generally warm.

In 2013, the authors in reference [14] numerically studied turbulent natural convection in a three-dimensional rectangular enclosure in the form of a room with a heater centrally fixed on the floor and two identical windows each fitted at the top of two opposite vertical walls. They considered a Boussinesq fluid motion in the enclosure. To enable the analysis of the flow and heat transfer rates, they discretized the set of non-dimensional equations governing a Newtonian fluid and the boundary conditions using the three-point central and forward difference approximations for non-uniform mesh. The resulting finite difference equations were then solved using numerical methods. The solutions were computed for $Re = 5500$ and $Pr = 0.71$. The results showed that the region at the middle of the room was warm while the regions near the windows were relatively cold. In 2015, the author in reference [15] used the robust finite volume method to investigate a steady two-dimensional laminar natural convection flow in a parallelogram shaped enclosure bounded by an adiabatic top wall, constant temperature cold sidewalls and a hot bottom wall at uniform temperature. He considered velocity components, pressure on a collocated grid as the dependent variables in the momentum equations, and used the SIMPLE algorithm to obtain the pressure field. The study considered Rayleigh number ranging from $10^3 \leq Ra \leq 10^5$ and $0.5 \leq AR \leq 1.5$. The results showed that the average Nusselt number increases as aspect ratio and Rayleigh number increases. In addition, he asserted that the aspect ratio of the flow domain is one of the parameters that determines the rate of heat transfer.

This paper aims at documenting the effects of varying the Rayleigh number on the distribution of the flow field of a Boussinesq turbulent natural convection airflow in an enclosure with adiabatic walls consisting of locally heated cooled sidewalls. Such flow conditions at high Rayleigh number and at constant aspect ratio are similar to many practical situations experienced in the real world.

2. Governing Equations

The principles of conservation of mass, momentum and energy expressed mathematically in form of differential equations govern non-turbulent and turbulent flow phenomena. Each equation contains a certain physical quantity as its dependent variable and implies a balance among all the quantities that influence this variable [16]. Since matter is continuously distributed in space, a fluid is considered as a continuum [17]. This concept allows us to express all the dependent variables and other flow quantities of the turbulent natural flow regime as continuous functions of space. Consequently, the equations governing the flow regime under study are anchored on the premise that

- The dynamic and chaotic behavior inherent in turbulent flow does not violate the conservation principles.
- The fluid is Newtonian and Boussinesq

- The fluid flow is buoyancy-driven and turbulent.
- The viscous dissipation effects in the energy equation are negligible.
- The heat transferred by conduction or radiation means is negligible.
- The only body force acting on the fluid is gravity.

Since the flow is Boussinesq, density is constant in the continuity equation and in all terms in the momentum equation except in the buoyancy term.

In a convective flow, a fluid of density ρ_0 displaces a fluid of density ρ where ρ_0 is the reference density of the fluid and ρ is the instantaneous fluid density. Thus, the net force F_b acting on a unit mass of the fluid is

$$F_b = (\rho_0 - \rho)gV \tag{1}$$

Where V is the volume of the fluid displaced. For a unit mass of the fluid,

$$V = \frac{1}{\rho_0} \tag{2}$$

Equation (2) thus becomes

$$F_b = \frac{(\rho_0 - \rho)}{\rho_0} g \tag{3}$$

Since temperature is the primary variable in heat transfer phenomena, it is imperative that we express the buoyant force in terms of temperature. We thus require a fluid property that measures the variation of density of the fluid with temperature. This property is the coefficient of volumetric expansion denoted as β . From definition, this coefficient is a measure of the rate of change of volume of a substance with temperature at constant pressure as shown in the equation below [2].

$$\beta = \frac{1}{V_0} \left(\frac{\partial V}{\partial T} \right)_p \tag{4}$$

For a unit mass of a fluid, density is inversely proportional to the volume, therefore

$$\frac{1}{V_0} \left(\frac{\partial V}{\partial T} \right)_p = -\frac{1}{\rho_0} \left(\frac{\partial \rho}{\partial T} \right)_p \tag{5}$$

Thus, at constant pressure

$$\beta = -\frac{1}{\rho_0} \left(\frac{\Delta\rho}{\Delta T} \right) \tag{6}$$

It then follows that

$$\beta = -\frac{1}{\rho_0} \frac{(\rho - \rho_0)}{(T - T_0)} \tag{7}$$

Hence,

$$\frac{\rho_0 - \rho}{\rho_0} = \beta [T - T_0] \tag{8}$$

Substituting equation (8) into (3) gives

$$F_b = g\beta [T - T_0] = \beta \Delta T g \tag{9}$$

From equation (9), it is apparent that the buoyancy force is dependent on the fluid properties and the temperature difference. Since the fluid properties are constant, buoyant force is purely a function of the temperature difference.

Considering a Boussinesq buoyant fluid flow with velocity component u_i in time t and spatial Cartesian coordinate x_i , the equations of continuity, momentum and energy respectively becomes ([19], [20], [21])

$$\frac{\partial u_i}{\partial x_i} = 0 \tag{10}$$

$$\frac{\partial u_i}{\partial t} + u_j \frac{\partial u_i}{\partial x_j} = -\frac{1}{\rho_0} \frac{\partial p}{\partial x_i} + \nu \frac{\partial^2 u_i}{\partial x_j^2} + g [\beta (T - T_0)] \tag{11}$$

$$\frac{\partial T}{\partial t} + u_i \frac{\partial T}{\partial x_i} = \frac{k}{\rho c_p} \frac{\partial^2 T}{\partial x_i^2} \tag{12}$$

Equations (10), (11) and (12), apply for both turbulent and non-turbulent flows.

2.1 Equations Governing the Turbulent Flow Field

Although turbulent flow at a given location in the flow field will satisfy equations (10) to (12) above, it is not feasible to resolve the enormous range of scales in space and time by direct numerical simulation. This is because the CPU requirements to do this exceeds by far the computing power for the most powerful computers available. Figure 1 below, shows the variation of a flow property with time in a turbulent flow field.

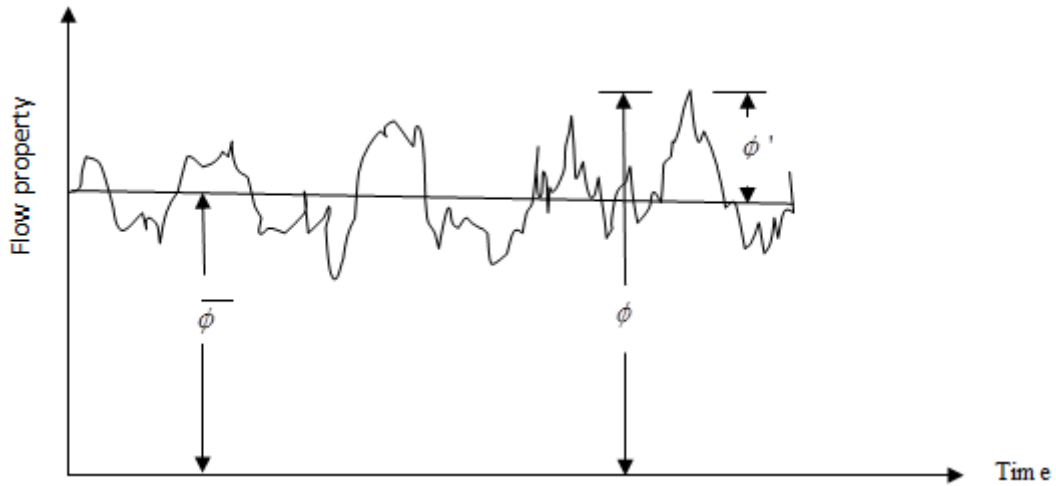


Figure 1: Time-variations of a flow property in a turbulent flow field

Since a flow property at a given point in the flow field exhibits a net mean behavior with small fluctuations about the mean value as a function of time, we subject equations (10) to (12) to the Reynolds decomposition and averaging process [16]. Accordingly, we express the flow variables as a sum of a mean and a fluctuation value such that

$$\phi(x,t) = \bar{\phi}(x) + \phi'(x,t) \quad (13)$$

where ϕ denotes the instantaneous value of the variable whereas $\bar{\phi}$ and ϕ' denotes the associated mean and fluctuation value respectively. The mean value is determined by taking the time average of the variable over a long period compared with the time scale of a typical fluctuation as expressed in the equation below

$$\bar{\phi} = \lim_{\Delta t \rightarrow \infty} \int_t^{t+\Delta t} \phi(x,t) dt \quad (14)$$

where Δt is the time averaging interval. Consequently, $\bar{\phi}$ does not change with time but with space. To incorporate the effects of turbulent fluctuations into the governing equations, we substitute the decomposed forms of the flow variables into equations (10) to (12) and then subject the resulting equations to the Reynolds rules of averaging to obtain

$$\frac{\partial \bar{u}_i}{\partial x_i} = 0 \quad (15)$$

$$\rho \left(\frac{\partial \bar{u}_i}{\partial t} + \bar{u}_j \frac{\partial \bar{u}_i}{\partial x_j} \right) = -\frac{\partial p}{\partial x_i} + g\rho \left[\beta_0 (\bar{T} - \bar{T}_0) \right] + \frac{\partial}{\partial x_j} \left[\mu \frac{\partial \bar{u}_i}{\partial x_i} - \overline{\rho u'_i u'_j} \right] \quad (16)$$

$$\rho c_p \frac{\partial \bar{T}}{\partial t} = -\frac{\partial}{\partial x_j} \left[-\kappa \frac{\partial \bar{T}}{\partial x_j} + \rho c_p \bar{u}_j \bar{T} + \overline{\rho c_p u'_j T'} \right] \quad (17)$$

The Reynolds-averaged equations (15) to (17) describes a turbulent flow field and the effect of the fluctuations on the flow. However, equation (16) and (17) contain unknown non-linear terms $\overline{\rho u'_i u'_j}$ and $\overline{\rho u'_j T'}$ respectively. These terms referred to as turbulent stresses and turbulent heat flux respectively represents the additional transfer of momentum and energy due to the fluctuations in the turbulent flow. There is need to find additional relations to determine these terms.

2.2 Determination of the Turbulence Quantities

Boussinesq asserted that there exist a linkage between the turbulent stresses and the mean rates of deformation. Moreover, from experimental evidence turbulent stresses increase with the mean rate of deformation [22]. Based on this assertions, the RANS turbulence models link the turbulent stresses and heat flux to the mean strain rate and temperature gradient respectively through an apparent viscosity μ_t and an apparent coefficient of conduction k_t . This idea referred to as the Boussinesq approximation leads to a relationship between turbulent stresses and the mean strain rate and between turbulent heat flux and temperature gradients as illustrated in equations (18) and (19) below [23].

$$\overline{\rho u'_i u'_j} = -\mu_t \left[\frac{\partial \bar{u}_i}{\partial x_j} + \frac{\partial \bar{u}_j}{\partial x_i} \right] + \frac{2}{3} \delta_{ij} \rho k \quad (18)$$

$$\overline{\rho u'_j T'} = -\frac{k_t}{c_p} \frac{\partial \bar{T}}{\partial x_j} \quad (19)$$

where k is the turbulent kinetic energy. However, both μ_t and k_t , unlike the laminar viscosity μ and thermal conductivity κ are not fluid properties but flow properties. However

$$k_t = \frac{\mu_t c_p}{Pr_t} \quad (20)$$

$$\mu_t = c_\mu \rho L \sqrt{k} \quad (21)$$

where k is the turbulent kinetic energy, L the turbulent length scale and C_μ an empirical constant determined experimentally [24].

In order to achieve closure, we require an equation for the determination of turbulent kinetic energy and another equation that allows the determination of the turbulent length scale.

2.2.1 Equation for Turbulent Kinetic Energy

This equation derived from the Navier-Stokes equation is of the form [25]

$$\underbrace{\rho \frac{\partial k}{\partial t}}_I + \underbrace{\rho \bar{u}_j \frac{\partial k}{\partial x_j}}_{II} = - \underbrace{\rho \bar{u}_i \bar{u}'_j \frac{\partial u_i}{\partial x_j}}_{III} - \underbrace{\beta g \rho \bar{u}' T'}_{IV} - \frac{\partial}{\partial x_j} \left[\underbrace{\frac{1}{2} \rho \bar{u}_i \bar{u}'_i \bar{u}'_j}_{V} + \underbrace{p \bar{u}'_j}_{VI} - \underbrace{\mu \frac{\partial k}{\partial x_j}}_{VII} \right] - \underbrace{\mu \frac{\partial \bar{u}'_i}{\partial x_j} \frac{\partial \bar{u}'_i}{\partial x_j}}_{VIII} \tag{22}$$

Each term in equation (22) represents an energy process occurring within the turbulent flow. Apart from terms I, II and $VIII$ representing the temporal, convection and molecular diffusion respectively, all other terms in the equation contains unknown correlations associated with the fluctuations in turbulent flow. Using similarity considerations coupled with the Boussinesq approximation, these terms are determined as below.

Applying the Boussinesq approximation, the production term III , denoted as P_k becomes

$$P_k = -\rho \bar{u}_i \bar{u}'_j \frac{\partial \bar{u}_i}{\partial x_j} = \mu_t \left[\frac{\partial \bar{u}_i}{\partial x_j} + \frac{\partial \bar{u}_j}{\partial x_i} \right] \frac{\partial \bar{u}_i}{\partial x_j} - \frac{2}{3} \delta_{ij} \rho k \frac{\partial \bar{u}_i}{\partial x_j} \tag{23}$$

However, from the equation of continuity, $\frac{\partial \bar{u}_i}{\partial x_j} = 0$. Equation (23) thus becomes

$$P_k = \mu_t \left[\frac{\partial \bar{u}_i}{\partial x_j} + \frac{\partial \bar{u}_j}{\partial x_i} \right] \frac{\partial \bar{u}_i}{\partial x_j} \tag{24}$$

Similarly, using equation (19), the buoyant generation term IV , denoted by G_k becomes

$$G_k = -\beta g \rho \bar{u}'_i T' = \beta g \frac{k_t}{c_p} \frac{\partial \bar{T}}{\partial x_i} \tag{25}$$

But

$$k_t = \frac{\mu_t c_p}{\sigma_k} \tag{26}$$

Thus

$$G_k = \beta g \frac{\mu_t}{\sigma_k} \frac{\partial \bar{T}}{\partial x_i} \tag{27}$$

where σ_k is the turbulent Prandtl number.

The turbulent diffusion term ν , is modeled using the gradient-diffusion law that assumes that kinetic energy diffuses down the gradient. The Fourier’s law of heat flux supports this assumption. According to this law, heat diffuses from hot to cold regions [2]. Applying this law, we obtain

$$\frac{1}{2} \overline{\rho u_i u_i u_j} = - \frac{\mu_t}{\sigma_k} \frac{\partial k}{\partial x_j} \tag{28}$$

The diffusion of turbulent kinetic energy due pressure gradient is small and consequently negligible. In addition, instead of modeling the turbulent dissipation term, an equation for its transport is developed.

Now using the modeled terms, we obtain the modeled equation for the transport of turbulent kinetic energy as

$$\rho \frac{\partial k}{\partial t} + \rho u_j \frac{\partial k}{\partial x_j} = \frac{\partial}{\partial x_j} \left[\left(\mu + \frac{\mu_t}{\sigma_k} \right) \frac{\partial k}{\partial x_j} \right] + P_k + G_k - \mu \frac{\partial u_i}{\partial x_j} \frac{\partial u_i}{\partial x_j} \tag{29}$$

2.2.2 Transport Equation for the Turbulent Dissipation Term

The turbulent dissipation term (ν) denoted as \mathcal{E} is dependent on the nature of the flow field that heavily relies on the descriptors of the large-scale motion, k and L .

The relation between these descriptors and the dissipation rate is as given in the equation below

$$\mathcal{E} = c_d \frac{k^{\frac{3}{2}}}{L} \tag{30}$$

where c_d is an empirical constant. Rearrangement of equation (30) gives

$$L = \frac{c_d k^{\frac{3}{2}}}{\varepsilon} \quad (31)$$

Substituting equation (31) into (21) results into

$$\mu_t = c_\mu \frac{\rho k^2}{\varepsilon} \quad (32)$$

From the author in reference [26]

$$\omega = \frac{\varepsilon}{c_\mu k} \quad (33)$$

where ω is the specific turbulent dissipation.

This implies that

$$\mu_t = \frac{\rho k}{\omega} \quad (34)$$

Since we already have the transport equation for k , we now need a transport equation for ω to achieve closure.

From the Wilcox formulation [26], the transport equation for ω is given as

$$\rho \frac{\partial \omega}{\partial t} + \rho \bar{u}_j \frac{\partial \omega}{\partial x_j} = \frac{\partial}{\partial x_j} \left[\left(\mu + \frac{\mu_t}{\sigma_\omega} \right) \frac{\partial \omega}{\partial x_j} \right] + \left[\beta - \frac{\kappa^2}{\sigma_\omega \sqrt{c_\mu}} \right] \rho \frac{\omega}{k} G_k - \rho \beta \omega^2 \quad (35)$$

Equations (29) and (35) provide the transport equations for the turbulent scalar quantities for the standard $k - \omega$ turbulence model.

However, on realizing the strengths and weaknesses of the standard turbulence models, Menter developed a blended model referred to as the Shear Stress Transport $k - \omega$ turbulence model to overcome the strong freestream sensitivity of the $k - \omega$ model and improve predictions of flow profiles in regions with adverse pressure [27]. He based its development on results of physical experiments conducted to reveal flow behavior for engineering applications.

The model which is a blend of the two standard turbulence models switches to the $k - \omega$ turbulence model in the inner regions of the boundary layer and transition regions, but switches to $k - \varepsilon$ turbulence model in the freestream regions. Therefore, in order to reveal the flow behavior in the entire flow domain, the *SST* $k - \omega$

turbulence model is the most appropriate model for resolving turbulence.

2.2.3 Transport Equations for the SST $k - \omega$ Turbulence Model

The SST $k - \omega$ turbulence model is a variant of the $k - \omega$ model obtained by expressing the $k - \varepsilon$ model in terms of k and ω resulting to an additional term in the transport equation for ω called the cross-diffusion term defined below

$$D_{\omega} = 2[1 - F_1] \rho \sigma_{\omega 2} \frac{1}{\omega} \frac{\partial k}{\partial x_j} \frac{\partial \omega}{\partial x_j} \quad (36)$$

The transport equations for this turbulence model are as given below [4].

Transport equation for turbulent kinetic energy k :

$$\rho \frac{\partial k}{\partial t} + \rho \bar{u}_i \frac{\partial k}{\partial x_i} = \frac{\partial}{\partial x_j} \left[\left(\mu + \frac{\mu_t}{\sigma_k} \right) \frac{\partial k}{\partial x_j} \right] + \rho G_k - \rho \beta^* \omega k \quad (37)$$

Transport equation for specific turbulent dissipation ω :

$$\rho \frac{\partial \omega}{\partial t} + \rho \bar{u}_i \frac{\partial \omega}{\partial x_i} = \frac{\partial}{\partial x_j} \left[\left(\mu + \frac{\mu_t}{\sigma_{\omega}} \right) \frac{\partial \omega}{\partial x_j} \right] + \gamma \rho \frac{\omega}{k} G_k + 2(1 - F_1) \rho \frac{\sigma_{\omega}}{\omega} \frac{\partial k}{\partial x_i} \frac{\partial \omega}{\partial x_i} - \rho \beta \omega^2 \quad (38)$$

The coefficients in the transport equations are blended forms of the coefficients of the standard $k - \varepsilon$ and $k - \omega$ models obtained using a blending function F_1 defined as

$$F_1 = \tanh[\phi_1^4] \quad (39)$$

where

$$\phi_1 = \min \left[\max \left(\frac{\sqrt{k}}{c_{\mu} \omega y}, \frac{500 \mu}{\rho \omega y^2} \right), \frac{4 \rho \sigma_{\omega 2} k}{CD_{K\omega} y^2} \right] \quad (40)$$

y is the normal distance to the wall and $CD_{K\omega}$ is the positive component of the cross-diffusion term defined as

$$CD_{K\omega} = \max \left[2 \rho \sigma_{\omega 2} \frac{1}{\omega} \frac{\partial k}{\partial x_i} \frac{\partial \omega}{\partial x_i}, 10^{-20} \right] \quad (41)$$

Accordingly, we obtain the coefficients present in the transport equations (40) and (41) using the relation

$$\varphi = \varphi_1 F_1 + \varphi_2 (1 - F_1) \quad (42)$$

where φ is the blended coefficient, φ_1 is a coefficient from the standard $k - \omega$ model while φ_2 is the corresponding coefficient from the standard $k - \varepsilon$ model.

2.2.4 The Final Set of the Governing Equations

From this point onwards, the upper-case letters will represent the mean-value component of the flow quantities while the lower-case letters will represent the corresponding fluctuation component. For temperature, T will represent the mean-value component while \mathbf{T} will represent the fluctuation component. Accordingly, the final set of the governing equations are:

Equation of Continuity

$$\frac{\partial U_i}{\partial x_i} = 0 \quad (43)$$

Equation of Momentum

$$\rho \left(\frac{\partial U_i}{\partial t} + U_j \frac{\partial U_i}{\partial x_j} \right) = -\frac{\partial P}{\partial x_i} + g \rho [\beta(T - T_0)] + \frac{\partial}{\partial x_j} \left[\mu \frac{\partial U_i}{\partial x_j} - \rho \overline{u_i u_j} \right] \quad (44)$$

Equation of Energy

$$\rho c_p \frac{\partial T}{\partial t} = -\frac{\partial}{\partial x_i} \left[-\kappa \frac{\partial T}{\partial x_j} + \rho c_p U_j T + \rho c_p \overline{u_j \mathbf{T}} \right] \quad (45)$$

Transport equation for turbulent kinetic energy

$$\rho \frac{\partial k}{\partial t} + \rho U_i \frac{\partial k}{\partial x_i} = \frac{\partial}{\partial x_j} \left[\left(\mu + \frac{\mu_t}{\sigma_k} \right) \frac{\partial k}{\partial x_j} \right] + \rho G_k - \rho \beta^* \omega k \quad (46)$$

Transport equation for specific dissipation rate

$$\rho \frac{\partial \omega}{\partial t} + \rho U_i \frac{\partial \omega}{\partial x_i} = \frac{\partial}{\partial x_j} \left[\left(\mu + \frac{\mu_t}{\sigma_\omega} \right) \frac{\partial \omega}{\partial x_j} \right] + \gamma \rho \frac{\omega}{k} G_k + 2(1 - F_1) \rho \frac{\sigma_\omega}{\omega} \frac{\partial k}{\partial x_i} \frac{\partial \omega}{\partial x_i} - \rho \beta \omega^2 \quad (47)$$

3. Mathematical Formulation

We consider a rectangular enclosure as the flow domain for simulating the Boussinesq turbulent natural convection flow. The physical set-up of the enclosure is as shown in the figure 2 below in which O is the origin of the rectangular Cartesian co-ordinates system and the axes are oriented as shown in the figure.

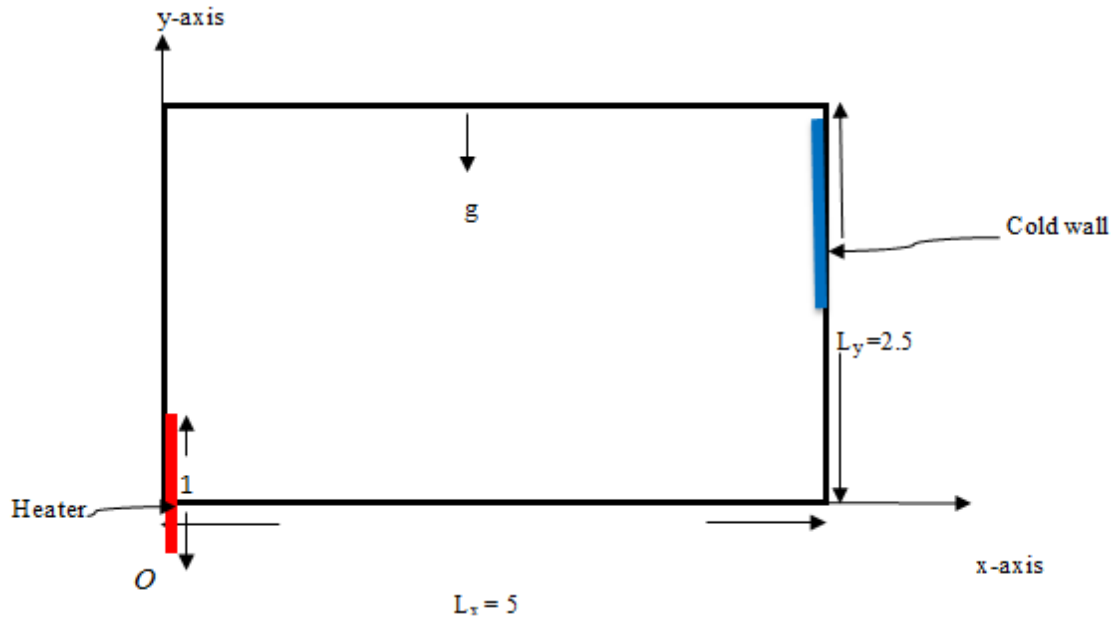


Figure 2: The physical set-up of the flow domain

The dimensionless geometrical configurations of the enclosure are $L_x = 5$, $L_y = 2.5$. It consists of a partially heated and cooled opposite vertical walls. The top and bottom walls of the enclosure and the unheated part of the vertical wall are adiabatic. Since heat transfer accompanies the flow, the characteristics of the flow field depend on the kinematic viscosity and thermal diffusivity of air. Kinematic viscosity is indicative of the amount of heat transported through molecular diffusion whereas thermal diffusivity is indicative of the amount of heat transported by conduction. Since thermal diffusivity and kinetic viscosity are both fluid properties, the distribution of the flow field is a function of the fluid properties. Since all the fluid properties are constant except for density variation in the buoyancy term, the ratio of the kinematic viscosity and thermal diffusivity of the fluid is a constant. This constant is the Prandtl number of the fluid defined as [2]

$$\text{Pr} = \frac{\nu}{\alpha} \tag{48}$$

The Prandtl number is thus indicative of the influence of the fluid properties on the flow field. The uniqueness of the flow is thus dependent on the flow conditions. The conditions influences the forces acting on the fluid and hence the heat transfer rate. In buoyancy-driven fluid flows, the Grashoff number provides a measure of the relative effect of the buoyant forces that initiates and sustains the flow and the forces opposing it. By definition, this non-dimensional number is the ratio of the product of the inertia force and buoyancy force to the square of

viscous force in a flow as illustrated in the equation below.

$$G_r = \frac{(Inertia\ force) \times (Bouyancy\ force)}{(Viscous\ force)^2}. \quad (49)$$

Therefore

$$G_r = \frac{(\rho U^2 L^2) \times (\rho \beta g \Delta T L^3)}{(\mu U L)^2} \quad (50)$$

Simplifying we obtain,

$$Gr = \frac{\rho^2 \beta g \Delta T L^3}{\mu^2} = \frac{\beta g \Delta T L^3}{\nu^2} \quad (51)$$

where L is the characteristic length of convection. Since β , g and ν are constants, the value of the Grashoff number is dependent on the temperature difference across the flow domain and is thus a flow property. The amount of heat transferred is thus dependent on both the Prandtl number of the fluid and the Grashoff number of the flow. Accordingly, the amount of heat transferred, measured using the Nusselt number is proportional to the Prandtl and Grashoff number.

$$Nu = f(Gr, Pr) = C(Gr.Pr)^a \quad (52)$$

From definition,

$$Ra = Gr.Pr. \quad (53)$$

Now substituting equation (48) and (51) into equation (53), we obtain

$$Ra = \frac{g \beta \Delta T L^3}{\nu \alpha} = \frac{\rho g \beta \Delta T L^3}{\mu \alpha} \quad (54)$$

This implies that the total amount of heat transferred is dependent of the Rayleigh number. Consequently, for a Boussinesq fluid flow in a confined flow domain of constant aspect ratio, we consider the Rayleigh number as the parameter that dictates the nature of the flow regime and the distribution of the associated flow profiles. Accordingly, the cold wall of the flow domain shown in figure 2 is maintained at a temperature of 10K while the temperature of the heated region is varied between $20K \leq \Delta T \leq 50K$ to obtain $10^9 \leq Ra < 10^{11}$. The Prandtl number of air is 0.71. The distribution of the flow profiles for $10^9 \leq Ra < 10^{11}$ is revealed by the distribution of the velocity and temperature contours in the Enclosure. For purposes of validation, the results

obtained for $Ra = 10^{10}$ are compared with the experimental results of Markatos and Pericleous. In fluid mechanics, a large number of numerical results are obtained through dimensional arguments. This is because the set of equations governing a fluid motion contains more variables than the number of equations. Consequently, there is need to reduce the number of variables in order to solve the equations. In addition, when we express the governing equations in non-dimensional form, the relative significance of the non-dimensional numbers in the flow is established [2]. We therefore non-dimensionalize equations (43) to (47) using a non-dimensional scheme that combines several dimensionless variables into non-dimensional numbers that are significant to the prevailing flow conditions. Since the main goal is to find the value of u_i and T_i at position x_i in the flow domain, each of the flow variables is non-dimensionalized using a characteristic dimensionless variable in respect to the non-dimensional scheme proposed by Lankhorst in which the characteristic velocity U_* is defined as [27]

$$U_* = \frac{\lambda_0}{\rho_0 c_{p_0} l_0} \tag{55}$$

We further select l_0 and T_* as the characteristic length and temperature respectively. All other flow variables are non-dimensionalized by their respective values at temperature T_* . Accordingly, we introduce the following non-dimensional scaling variables in which the superscript prime denotes the non-dimensional quantities, the subscript star denotes a variable defined in respect to the non-dimensional scheme and the subscript 0 denotes the variables evaluated at a reference state. The mean value and the corresponding fluctuating component of a variable share the same scaling variables

$$x'_i = \frac{x_i}{l_0}, \quad U'_i = \frac{U_i}{U_*}, \quad v'_i = \frac{v_i}{v_0}, \quad \theta = \frac{T - T_*}{\Delta T_*}, \quad \rho' = \frac{\rho}{\rho_0}, \quad k' = \frac{k}{U_*}, \quad p' = \frac{p}{p_0}, \quad \mu' = \frac{\mu}{\mu_0}, \quad t' = t \frac{U_*}{l_0}$$

$$g' = \frac{g}{g_0} \tag{56}$$

Using this scheme the non-dimensional form of equations (43) to (47) respectively becomes

$$\frac{\partial U_i}{\partial x_i} = 0 \tag{57}$$

$$\frac{\partial U_i}{\partial t} + U_j \frac{\partial U_i}{\partial x_j} = - \left(\frac{Ra Pr^2}{\xi_\eta} \right)^{2/3} \frac{Pn}{Gn} \frac{1}{\rho} \frac{\partial P}{\partial x_i} + \left(\frac{Ra Pr}{\xi_\eta} \right) (\beta \theta \Delta T_*) +$$

$$\frac{\partial}{\partial x_j} \left[Pr v \frac{\partial U_i}{\partial x_j} - \overline{u_i u_j} \right] \tag{58}$$

$$\rho c_p \frac{\partial \theta}{\partial t} = - \frac{\partial}{\partial x_i} \left[Pn \xi^{-1} \kappa \frac{\partial \theta}{\partial x_i} + \rho c_p U_i \theta + \rho c_p \overline{u_i \theta} \right] \quad (59)$$

$$\rho \frac{\partial k}{\partial t} + \rho U_j \frac{\partial k}{\partial x_j} = Pr \frac{\partial}{\partial x_i} \left[\left(\mu + \frac{\mu_t}{\sigma_k} \right) \frac{\partial k}{\partial x_i} \right] + \frac{Ra Pr}{\xi_\eta} \rho G_k - \rho \beta^* \omega k \quad (60)$$

$$\rho \frac{\partial \omega}{\partial t} + \rho U_j \frac{\partial \omega}{\partial x_j} = Pr \frac{\partial}{\partial x_i} \left[\left(\mu + \frac{\mu_t}{\sigma_\omega} \right) \frac{\partial \omega}{\partial x_i} \right] + \frac{Ra Pr}{\xi_\eta} \gamma \rho \frac{\omega}{k} G_k - \beta \rho \omega^2 + \frac{1}{Gn} \left[\frac{Ra Pr^2}{\xi_\eta} \right]^{2/3} 2(1 - F_1) \frac{\sigma_\omega}{\omega} \frac{\partial k}{\partial x_i} \frac{\partial \omega}{\partial x_i} \quad (61)$$

For the remainder of this paper, all variables and equations referenced are non-dimensional.

3.1 The Boundary Conditions

In order to complete the mathematical formulation, we specify the boundary conditions of the field variables present in the governing equations.

3.1.1 Temperature boundary conditions

For a bounded solution, we bound the non-dimensional temperature $\theta = \frac{T - T_*}{\Delta T_*}$ within the flow domain. We

conveniently choose $T_* = T_c$ so that on the heated region, $T = T_h$ hence,

$$\theta = \frac{T_h - T_c}{\Delta T_*} = \frac{T_h - T_c}{T_h - T_c} = 1. \quad (62)$$

On the cold region, $T = T_c$ hence

$$\theta = \frac{T_c - T_*}{\Delta T_*} = \frac{T_c - T_c}{T_h - T_c} = 0. \quad (63)$$

Thus within the flow domain $0 \leq \theta \leq 1$. The walls of the flow domain are adiabatic, thus taking n as a scalar of the outward unit vector normal to the walls,

$$\frac{\partial \theta}{\partial n} = 0. \quad (64)$$

3.1.2 Velocity boundary conditions

The walls of the flow domain are stationary and impermeable. We specify the state of the fluid motion at the boundaries in terms of the velocity of the fluid particles. The non-slip velocity boundary condition apply on all the bounding surfaces of the flow domain as outlined below.

$$u(x=0, y) = v(x=0, y) = 0 \tag{65}$$

$$u(x=L_x, y) = v(x=L_x, y)=0 \tag{66}$$

$$u(x, y=0) = v(x, y=0) = 0 \tag{67}$$

$$u(x, y=L_y) = v(x, y=L_y)=0 \tag{68}$$

However, the pressure field is not specified since it is deduced from the velocity field.

4. Method of solution

The finite volume method is used to discretize the computational domain and the governing equations. The method possesses the ability to adapt a grid structure that captures the local features of the flow domain and the final form of the discretized equations has an intimate connection to the actual physical situation. To ensure that the conservation laws are satisfied at both the local and global level, the method takes the quantity balance of each dependent variable at each node of the computational domain. Accordingly, based on the assumption that a piecewise profile describing the variation of the dependent variable across neighbouring nodes exist, the solution domain is decomposed into a union of non-overlapping finite volumes whose centroids are the computational nodes [16]. One generic conservation equation that comprises of all physical processes of transporting a quantity is imposed in each of the finite volumes in its integral form [17]. We thus express the equations (57) to (61) in a conservative compact form as

$$\frac{\partial X}{\partial t} + \frac{\partial \chi}{\partial x_j} = S \tag{69}$$

where

$$X = \begin{bmatrix} 0 \\ U_i \\ \rho c_p \theta \\ \rho k \\ \rho \omega \end{bmatrix},$$

$$\chi_i = \begin{bmatrix} U_i \\ U_i U_j + \zeta p - P_r \nu \frac{\partial U_i}{\partial x_j} + \overline{u_i u_j} \\ \mathcal{G} \frac{\partial \theta}{\partial x_i} + \rho c_p (U_i \theta + \overline{u_i \theta}) \\ \rho k U_j + P_r d_j^{(k)} \\ \rho \omega U_j + P_r d_j^{(\omega)} \end{bmatrix}$$

$$S = \begin{bmatrix} O \\ \zeta S^m \\ O \\ S^{(k)} \\ S^{(\omega)} \end{bmatrix}$$

$$\zeta = \left(\frac{R_a P_r^2}{\xi_\eta} \right)^{2/3} \frac{P_n}{G_n} \frac{1}{\rho}, \quad \mathcal{G} = P_n \xi^{-1} \kappa \quad \text{and} \quad \zeta = \frac{R_a P_r}{\xi_\eta}.$$

\mathbf{X} is the state vector to be determined, χ_i is a vector for the flux terms and S represents the source terms. These vectors consists of the dependent variables defined at the computational nodes. The first term of each of the vectors and the source term correspond to the continuity equation while the second terms in all the vectors correspond to the momentum equation. The third terms correspond to the energy equation while the fourth and fifth terms respectively correspond to the transport equations for turbulent scalar quantities. We define the source term $S^{(m)}$, the diffusion terms $d^{(k)}$, $d^{(\omega)}$ in the momentum, and the source terms $S^{(k)}$, $S^{(\omega)}$ present in the transport equations for k and ω as

$$S^{(m)} = \beta \theta \Delta T \tag{70}$$

$$d_j^{(k)} = \frac{\partial}{\partial x_j} \left\{ \left[\mu + \frac{\mu_t}{\sigma_k} \right] \frac{\partial k}{\partial x_j} \right\} \tag{71}$$

$$d_j^{(\omega)} = \frac{\partial}{\partial x_j} \left\{ \left[\mu + \frac{\mu_t}{\sigma_\omega} \right] \frac{\partial \omega}{\partial x_j} \right\} \tag{72}$$

$$S^{(k)} = \frac{R_a P_r}{\xi_\eta} \rho G_k - \rho \beta * \omega k \tag{73}$$

$$S^{(\omega)} = \frac{R_a P_r}{\xi_\eta} \gamma \rho \frac{\omega}{k} G_k - \beta \rho \omega^2 + \frac{1}{G_n} \left[\frac{R_a P_r^2}{\xi_\eta} \right]^{2/3} 2(1 - F_1) \frac{\sigma_\omega}{\omega} \frac{\partial k}{\partial x_i} \frac{\partial \omega}{\partial x_i} \quad (74)$$

Since equation (69) contains all the processes involved in the transport of a quantity in the flow field, we express it as generalized transport equation for the dependent variable ϕ of the form [28]

$$\frac{\partial}{\partial t} \rho \phi + \left[\frac{\partial}{\partial x_j} (\rho u_j \phi) - \frac{\partial}{\partial x_j} \left(\Gamma_\phi \frac{\partial}{\partial x_j} \phi \right) \right] = S_\phi \quad (75)$$

where Γ_ϕ is the exchange coefficient of ϕ and S_ϕ is its source. Equation (75) contain four distinct terms. The first term on the left shows the change of the variable with time; the second term shows the advection of the variable with the flow whereas the third term shows the diffusion of the quantity. Both the second and third term thus represent the flux of ϕ across the boundaries of the finite volume. The term on the right hand side shows the source of the quantity. Consequently, the rate of change of ϕ in a finite volume with respect to time is equal to the sum of the net flux of ϕ due to convection into the finite volume, the net flux of ϕ due to diffusion into the finite volume and the generation rate of ϕ inside the finite volume [17]. The equation thus incorporates all the transport processes of a quantity and hence represents the flux balance in a finite volume. Therefore, by sequentially setting ϕ to $1, u, v, w, T, k, \omega$ and with the appropriate values of Γ_ϕ and S_ϕ , the equation of continuity, momentum, energy and the turbulent equations can all be written in the form of equation (75).

Integrating equation (75) over the finite volume, we obtain

$$\frac{\partial}{\partial t} \int_V \rho \phi dV + \int_V \frac{\partial}{\partial x_j} (\rho u_j \phi) dV - \int_V \frac{\partial}{\partial x_j} \left(\Gamma_\phi \frac{\partial}{\partial x_j} \phi \right) dV = \int_V S_\phi dV . \quad (76)$$

Using the Gauss's divergence theorem, we convert the volume integrals in equation (76) into integrals over the entire surface S bounding the finite volume to obtain

$$\frac{\partial}{\partial t} \int_V (\rho \phi) dV + \left[\int_S (\rho \phi u) ds - \left(\Gamma_\phi \frac{\partial}{\partial x_j} \phi \right) ds \right] = \int_V S_\phi dV \quad (77)$$

The integrals are discretized using the finite volume method to obtain a system of algebraic equations of the form

$$a \phi + \sum_{nb} a_{nb} \phi_{nb} = b \quad (78)$$

The coefficient a contains the contributions of all the terms corresponding to ϕ . The coefficient a_{nb} contain the corresponding contributions of each of the neighbouring finite volumes whereas the coefficient b contains the contributions of the source terms.

The SIMPLER algorithm is used to obtain the pressure field. Since each finite volume provides one equation for each dependent variable, we obtain an equation set for each finite volume. However, these equations are coupled in sense that the coefficients in the equations depend on the previous values of the dependent variables; the coefficients are thus a function of the solution. Consequently, we use an iterative segregated pressure-based solver built in Fluent 16.0 that solves equations sequentially for each dependent variable.

In each equation, the unknown is assumed to be a single field variable and hence the equation is solved without regard to the solution of other field variables. In order to improve the stability of the iteration process, we use under-relaxation factors to lower the variations of the dependent variable from one iteration to the next. The absolute residual measure of ϕ at a point in the computational domain is obtained using the equation below.

$$R = \left| a\phi - \sum_{nb} a_{nb}\phi_{nb} - b \right| \tag{79}$$

In every iteration, the value of the coefficients a_{nb} and b changes in each finite volume. The overall measure of the scaled residual in the entire computational domain thus becomes

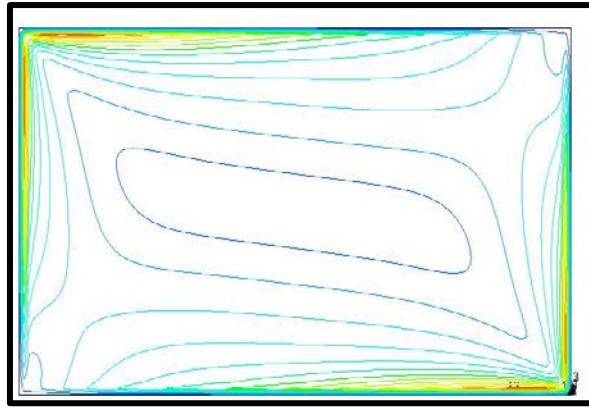
$$R^\phi = \frac{\sum_{all\ cells} \left| a\phi - \sum_{nb} a_{nb}\phi_{nb} - b \right|}{\sum_{all\ cells} |a\phi|} \tag{80}$$

For convergence, we set $R^\phi \leq 10^{-6}$.

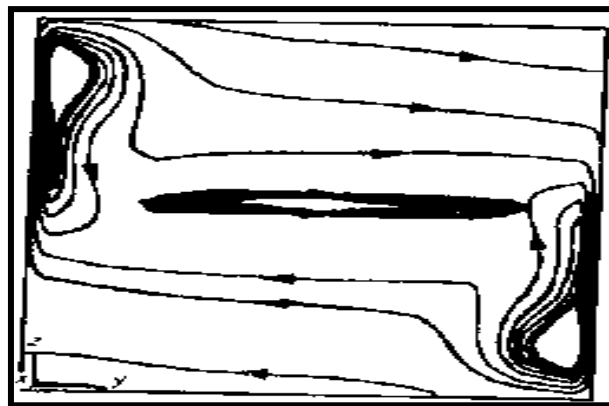
5. Results and discussions

The distribution of the velocity and temperature fields in the enclosure is determined for $10^9 \leq Ra < 10^{11}$ at $AR = 0.5$. The distribution of velocity and temperature contours reveals the flow fields. For validation purposes, we compare the results obtained at $Ra = 10^{10}$ with the experimental results of Markatos and Pericleous.

Figures 3 and 4 below respectively shows a comparison between the distribution of the velocity and temperature contours obtained in the current study at $Ra = 10^{10}$ and the experimental results at the same Rayleigh number [29].

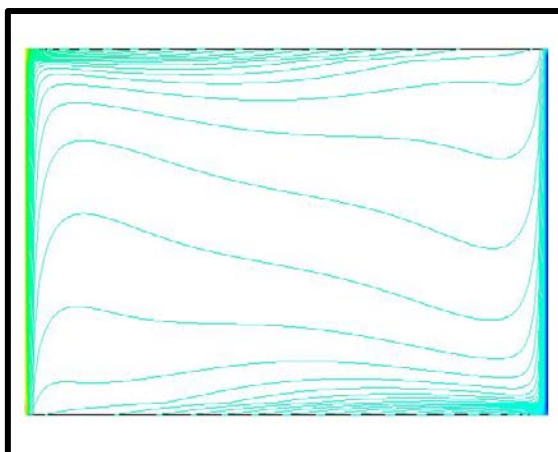


Current results

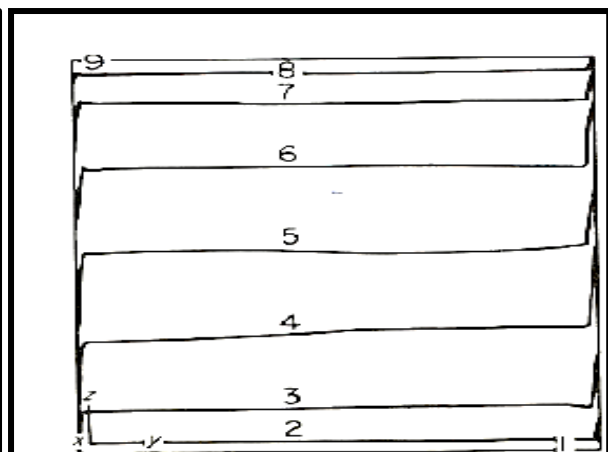


Markatos and Pericleous experimental results

Figure 3: The distribution of velocity field at



Current results



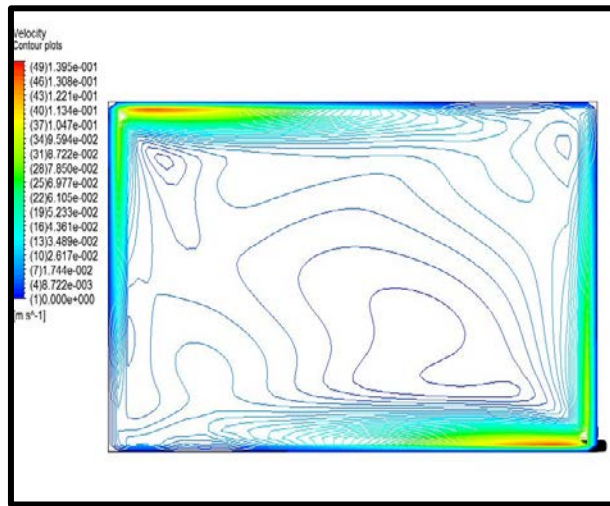
Markatos and Pericleous experimental results

Figure 4: The distribution of the temperature field at

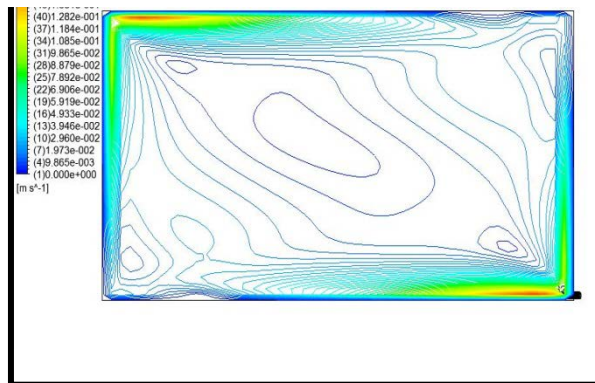
From figure 3, both results reveals the presence of recirculating vortices in the central region of the flow domain. It is also apparent from both results that velocity in the upper left and lower right regions of the flow domain is higher than the upper right and lower left regions. In addition, the results shows that the flow velocity is high in the regions near the heater and the cold patch while the interior is virtually stagnant. In both cases, the distribution of the velocity contours in the flow domain agree considerably. From figure 4, the alignment of temperature contours in both cases are similar. In addition, the temperature of the contours decrease gradually from the upper region of the flow domain to the lower side in both cases. Therefore, both results indicate that the flow domain is thermally stratified. The results further reveals the existence of high temperature gradients along the vertical walls. This due to the effects of the buoyant forces. The current results are therefore consistent with the experimental results.

5.1 The Distribution of Velocity fields at Varying Rayleigh Number

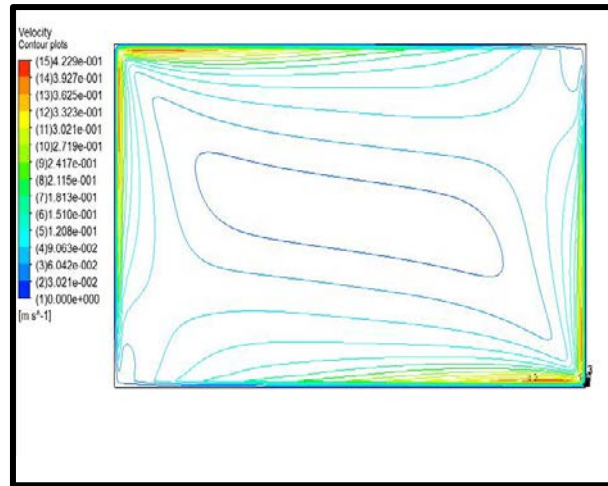
The effect of the Rayleigh on the velocity field is revealed by the distribution of the velocity contours in the enclosure at various Rayleigh number as shown in Figure 5 below. The magnitude of velocity along the contours is as shown on the scale bar to the left of each distribution.



$Ra = 9.131 \times 10^9, AR = 0.5$



$Ra = 2.739 \times 10^{10}, AR = 0.5$



$$Ra = 5.479 \times 10^{10}, \quad AR = 0.5$$

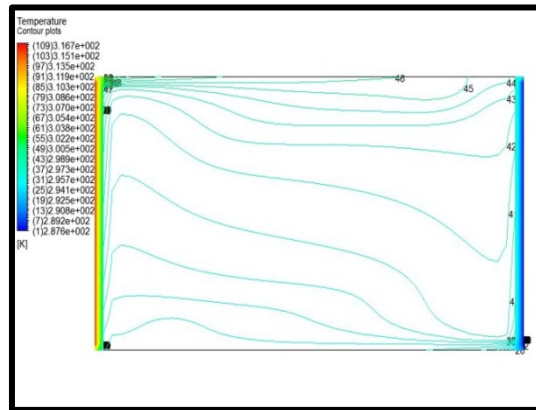
Figure 5: The distribution of the velocity field at varying Rayleigh number

From the results, it is evident that the distribution of velocity in the enclosure and the thickness of boundary layer varies with the Rayleigh number. The variation in velocity is in both the magnitude and location of the recirculating vortices. When the Rayleigh number is $Ra = 9.131 \times 10^9$, the results reveal that the convection currents are very intense on the upper left and lower right corners of the enclosure while the interior region is virtually stagnant. As the Rayleigh number increases, the distribution and magnitude of velocity changes significantly as demonstrated by the alignment of the contours. Since the value of the Rayleigh number is a function of the temperature difference, the magnitude of velocity in the entire enclosure increases with increase in the temperature difference. However, although the size of the stagnant region in the interior of the enclosure reduces significantly with increase of the Rayleigh number, the velocities in the upper and lower regions of the enclosure are generally higher than in the interior region. In addition, the location of the circulating vortices changes with increase in the Rayleigh number. When $Ra = 9.131 \times 10^9$, there are three recirculating vortices of different sizes and at different locations of the enclosure. Two of the vortices are located on the upper side of the enclosure and the third on the lower side. As the Rayleigh number increases to $Ra = 2.739 \times 10^{10}$, the vortices on the upper side enlarges significantly and stretches towards the center of the enclosure while the one on the lower side shrinks and shifts towards the lower right corner of the enclosure. At $Ra = 5.479 \times 10^{10}$, the center of most of the recirculating vortices is about the center of the enclosure. This is a demonstration of velocity stratification in the enclosure. Further increase in the Rayleigh number makes this stratification more pronounced. The velocity of the contours adjacent to the walls of the enclosure is zero at all values of the Rayleigh number. However, the thickness of this layer reduces gradually as the Rayleigh increases. This is due to the increase of the strength of the buoyant force causing the air particles held by adhesive forces to move with the current. However, this layer is slightly thicker along the horizontal walls than along the vertical walls.

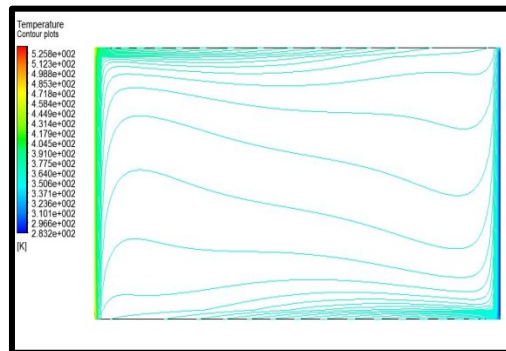
5.2 The Distribution of Temperature Field at Varying Rayleigh Number

The distribution of the temperature profiles and the effect of varying the Rayleigh number on this distribution is

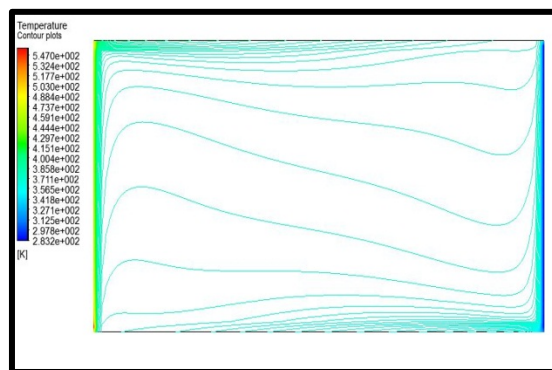
as depicted by the distribution of the temperature contours in the enclosure at different values of the Rayleigh numbers as shown in figure 6 below. The temperature along the contours is as indicated on the scale bar to the left of each distribution.



(a): $Ra = 9.131 \times 10^9$, $AR = 0.5$



(b): $Ra = 2.739 \times 10^{10}$, $AR = 0.5$



(c): $Ra = 5.479 \times 10^{10}$, $AR = 0.5$

Figure 6: The distribution of temperature field at varying Rayleigh number

From the above results, it is evident that the distribution of temperature field is dependent of the Rayleigh

number of the flow as revealed by the alignment of the contours in the enclosure at different values of the Rayleigh number. As the Rayleigh number increases, the vertical distance between successive maximum points of the contours gradually reduce upwards while the vertical distance between successive minimum points gradually increase downwards. This causes a high concentration of the contours on the upper left and lower right corners of the enclosure. These regions are thus experiencing stronger buoyancy forces due to the high temperature gradients. It is also apparent that the contours are very close along the vertical walls of the enclosure showing that the bulk of the flow and energy transfer is concentrated within the regions adjacent to the heater and the cold wall. Generally, the upper region of the enclosure is at higher temperature than the lower region. The enclosure is thus thermally stratified.

6. The Conclusion

- In a locally heated enclosure of constant aspect, the magnitude and distribution of the flow field is dependent of the Rayleigh number of the flow.
- The thickness of the boundary layer reduces as the Rayleigh increases.

Therefore, the thermal state in a locally heated enclosure of constant aspect is dependent of the Rayleigh number.

7. Recommendation for further studies

- Effect of the Prandtl number on the distribution of the turbulent flow field in an enclosure.
- Distribution of flow field in respect to the position of the heater and sink.

References

- [1] M. Aounallah, Y. Addad, S. Benhamadouche, O. Imine, L. Adjlout and D. Laurence, "Numerical investigation of turbulent natural convection in an inclined square enclosure with a hot wavy wall," 2007.
- [2] R. K. Rajput, Heat and Mass Transfer: A Textbook for the Students Preparing for B.E., B.Tech., B.Sc. Engg, AMIE, UPSC (Engg. Services) and GATE Examinations, S. Chand Limited, 2015.
- [3] B. E. Launder and D. B. Spalding, "The numerical computation of turbulent flows," Computer Methods in Applied Mechanics and Engineering, vol. 3, pp. 269-289, 1974.
- [4] F. R. Menter, "Two-equation eddy-viscosity turbulence models for engineering applications," AIAA Journal, vol. 32, pp. 1598-1605, #aug# 1994.
- [5] P. K. Kundu and I. M. Cohen, Fluid Mechanics., Elsevier Science, 2001, p. 755.
- [6] H. Ozoe, A. Mouri, M. Ohmuro, S. W. Churchill and N. Lior, "Numerical calculations of laminar and turbulent natural convection in water in rectangular channels heated and cooled isothermally on the

opposing vertical walls," *International Journal of Heat and Mass Transfer*, vol. 28, pp. 125-138, 1985.

- [7] H. Ozoe, A. Mouri, M. Hiramitsu, S. W. Churchill and N. Lior, "Numerical Calculation of Three-Dimensional Turbulent Natural Convection in a Cubical Enclosure Using a Two-Equation Model for Turbulence," *Journal of Heat Transfer*, vol. 108, pp. 806-813, nov 1986.
- [8] M. November and M. W. Nansteel, "Natural convection in rectangular enclosures heated from below and cooled along one side," *International Journal of Heat and Mass Transfer*, vol. 30, pp. 2433-2440, 1987.
- [9] D. Sadowski, D. Poulikakos and M. Kazmierczak, "Three-Dimensional Natural Convection Experiments in an Enclosure," *Journal of Thermophysics and Heat Transfer*, vol. 2, pp. 242-249, jul 1988.
- [10] G. De Vahl Davis, E. Leonard and S. A. Wong, "Three-dimensional natural convection in a room," 1988.
- [11] F. K. Gatheri, J. A. Reizes, E. Leonardi and G. De Vahl Davis, "Natural Convection in a Rectangular Enclosure with Colliding Boundary Layers: Numerical study," *Proceedings 5th Australasian Heat and Mass Conference*, pp. 69.1-69.6, 1993.
- [12] O. Aydin and W.-J. Yang, "Natural convection in enclosures with localized heating from below and symmetrical cooling from sides," *International Journal of Numerical Methods for Heat & Fluid Flow*, vol. 10, pp. 518-529, 2000.
- [13] J. K. Sigey, F. K. Gatheri and M. Kinyanjui, "Numerical study of free convection turbulent heat transfer in an enclosure," *Energy Conversion and Management*, vol. 45, pp. 2571-2582, 2004.
- [14] O. E. Mairura, J. K. Sigey, J. A. Okello and J. M. Okwoyo, "Natural Convection with Localized Heating and Cooling on Opposite Vertical Walls in an Enclosure," *The SIJ Transactions on Computer Networks & Communication Engineering (CNCE)*, 2013.
- [15] E. A. Salih, "Effects of Aspect Ratio on Natural Convection Heat Transfer in a Parallelogrammic Enclosure Heated from Below," *ZANCO Journal of Pure and Applied Sciences*, vol. 27, pp. 45-56, 2015.
- [16] S. Patankar, *Numerical Heat Transfer and Fluid Flow*, Taylor & Francis, 1980.
- [17] J. F. Douglas, J. M. Gasiorek, J. A. Swaffield and L. B. Jack, *Fluid Mechanics*, Pearson/Prentice Hall, 2005.
- [18] J. Boussinesq, *Theorie analytique de la Chaleur*, Gauthier-Villars, 1903.

- [19] J. Anderson, Computational Fluid Dynamics, McGraw-Hill Education, 1995.
- [20] R. h. Pletcher, J. C. Tannehill and D. Ander, Computational Fluid Mechanics and Heat Transfer, New York: Taylor and Francis, 1997.
- [21] I. G. Currie, Fundamental Mechanics of Fluids, Fourth Edition, Taylor & Francis, 2012.
- [22] H. K. Versteeg and W. Malalasekera, An Introduction to Computational Fluid Dynamics: The Finite Volume Method, Pearson Education Limited, 2007.
- [23] L. Davidson, An Introduction to Turbulence Models, Chalmers University of Technology, 2011.
- [24] W. Rodi, Turbulence Models and Their Application in Hydraulics, Taylor & Francis, 1993.
- [25] H. Tennekes and J. L. Lumley, A First Course in Turbulence, Pe Men Book Company, 1972.
- [26] D. C. Wilcox and others, Turbulence modeling for CFD, vol. 2, DCW industries La Canada, CA, 1998.
- [27] A. M. Lankhorst and A. Marinus, "Laminar and turbulent convection in cavities: Numerical modeling and experimental validation," Ph.D. Thesis Technische Univ., Delft (Netherlands), 1991.
- [28] F. T. Pinho, "The Finite-volume Method Applied to Computational Rheology: II-Fundamentals for Stress-explicit Fluids," University of Porto, vol. 1, pp. 63-100, 2001.
- [29] N. C. Markatos and K. A. Pericleous, "Laminar and turbulent natural convection in an enclosed enclosure," International Journal of Heat and Mass Transfer, vol. 27, pp. 755-772, 1984.

Appendix

Nomenclature

Roman Symbols

AR	Aspect ratio of the flow domain
a_{nb}	Coefficients of the neighbouring finite volumes
C_p	Specific heat capacity at constant pressure
C_μ	Empirical turbulence constant
C_D	Cross-diffusion term

C_d	An empirical constant
$c_{\varepsilon 1}, c_{\varepsilon 2}$	Model constants
F	External body force per unit volume
F_b	Buoyancy force per unit volume
F_1, F_2	Blending functions
g	Acceleration due to gravitational
k	Turbulent Kinetic energy
k_t	Turbulent coefficient of conduction
G_k	Buoyant production of turbulent kinetic energy
P_k	Shear production of turbulent kinetic energy
L_0	Characteristic length of the convection
P	Thermodynamic Pressure
T	Thermodynamic Temperature
T_*	Characteristic Temperature
ΔT	Temperature difference
t	Time
Δt	Time interval
u_i	Instantaneous velocity components
U_i	Mean velocity components

U_*	Characteristic velocity
i, j	Unit vectors in the x, y directions respectively
L_x, L_y	Dimensionless lengths of the flow domains in the x, y directions respectively
S	Source term
d	Diffusion term
n	Normal vector
R	Residual measure
Pr	Prandtl number
Ra	Rayleigh number
Gr	Grashof number
Nu	Nusselt number
Gn	Gravity number

Greek Symbols

α	Thermal diffusivity
β	Co-efficient of volumetric expansion
ρ	Density of fluid
ω	Dissipation rate per unit of turbulent kinetic energy
μ	Dynamic viscosity of the fluid
μ_t	Turbulent viscosity
λ	Thermal conductivity

θ	Non-dimensional temperature
ε	Dissipation rate of turbulent kinetic energy
ϕ	A flow-field variable
φ	Blended coefficients
γ_k, γ_ω	Dissipation rate of k and ω respectively
κ	Coefficient of thermal conductivity of the medium
χ_i	Flux vector
ξ	Non-dimensional temperature difference
∂	Differential operator
σ_k	Turbulent Prandtl number for k

Subscripts

0	Reference state
h	Heater
t	Turbulent
nb	Neighbor
*	Characteristic value

Superscripts

—	Mean value
'	Fluctuating component
.	Non-dimensional quantity

t	Time
m	Momentum equation
k	Turbulent kinetic energy equation
ω	Specific dissipation rate Equation

Acronyms

SIMPLER	SIMPLE Revised
CPU	Computer Processing Unit